Fast Adsorption of Soft Hydrogel Microspheres on Solid Surfaces in Aqueous Solution

Shusuke Matsui,[a] Takuma Kureha,[a] Seina Hiroshige,[a] Mikihiro Shibata,[c] Takayuki Uchihashi,*[, d] and Daisuke Suzuki*[, a], [b]

Abstract: The real-time adsorption behavior of polymeric colloidal microspheres onto solid surfaces in aqueous solution was visualized for the first time using high-speed atomic force microscopy (HS-AFM) in order to reveal how the softness of the microspheres affects their dynamic adsorption. Studies that focus on the deformability of microspheres upon dynamic adsorption have not yet been reported, most likely on account of a lack of techniques that appropriately depict the dynamic adsorption and deformation behavior of individual microspheres at the nanoscale in real time. In this study, we revealed that the deformability of microspheres plays a crucial role on the adsorption kinetics, i.e., soft hydrogel microspheres adsorb faster than harder elastomeric or rigid microspheres. The results of this study should provide insight towards development of new colloidal nanomaterials that exhibit effective adsorption on specific sites in aqueous solution.

Upon colliding with a rigid surface, a spherical object either rebounds or adheres, and the specific behavior of a particular object is determined by its reflection coefficient. On the microscopic scale, colloidal microspheres can also engage in contact with and adsorb onto solid surfaces in aqueous solution. These phenomena are highly important in an industrial or biological context, for e.g. the coating of solid surfaces with colloidal microspheres, and the adsorption of blood platelets onto injured regions in blood vessels, which stops bleeding. In terms of pharmaceutical applications, drug delivery vehicles consisting of artificial polymeric microspheres have to effectively adsorb onto diseased sites for an effective transportation of drugs. Hence, the understanding of the contact and adsorption phenomena of microspheres is important for the development of advanced colloidal nanomaterials. Theoretically, the adsorption of rigid colloidal microspheres onto solid surfaces is dominated by electrostatic and van der Waals interactions.[1]

[a] S. Matsui, S. Hiroshige, T. Kureha, Prof. Dr. D. Suzuki
Graduate School of Textile Science & Technology, Shinshu University
3-15-1 Tokida Ueda, Nagano 386-8567, Japan

[b] Prof. Dr. D. Suzuki
Division of Smart Textile, Institute for Fiber Engineering, Interdisciplinary Cluster for Cutting Edge Research, Shinshu University
3-15-1 Tokida Ueda, Nagano 386-8567, Japan
E-mail: d_suzuki@shinshu-u.ac.jp

[c] Prof. Dr. M. Shibata
High-speed AFM for Biological Applications Unit, Institute for Frontier Science Initiative, Kanazawa University, and Bio-AFM Frontier Research Center, Kanazawa University
Kakuma-machi, Kanazawa 920-1192, Japan

[d] Prof. Dr. T. Uchihashi
Department of Physics and Structural Biology Research Center, Graduate School of Science, Nagoya University
Furo-cho, Chikusa-ku, Nagoya, Aichi 464-8602, Japan
E-mail: uchihast@d.phys.nagoya-u.ac.jp

Supporting information for this article is given via a link at the end of the document.

However, the process that occurs between the microspheres and the surface at the moment of physical contact is poorly understood.[2] Especially as colloidal microspheres usually exhibit at least some degree of elasticity (deformability), the microspheres can be subject to deformation upon contact with solid surfaces. The deformability plays an important role for their biological functionality, e.g. their biodistribution and circulation times.[3] Such adsorption or deformation of the microspheres on solid surfaces have so far been investigated by atomic force microscopy (AFM) and so forth.[4] However, to the best of our knowledge, how this deformability affects the dynamic contact and adsorption behavior of the microspheres onto the surface has not yet been addressed, due to the difficulties associated with the direct visualization of the dynamic adsorption and deformation behavior of individual microspheres at the nanoscale in real time.

Against this background, we visualized individual microspheres during their adsorption and subsequent deformation, and discovered that the deformability of individual microspheres strongly impacts the adsorption kinetics. This approach, which enabled us to monitor the moment of adsorption and deformation of individual microspheres, was realized by high-speed atomic force microscopy (HS-AFM).[5] This method allows the direct visualization of the structural dynamics of biological molecules in action, without significantly disturbing the physiological function of the molecules.[4] In this study, we have applied HS-AFM techniques to artificial polymeric microspheres with different softness as model colloids under liquid conditions, and investigated the relationship between the adsorption kinetics and the elasticity of the microspheres that adsorb onto solid substrates.

The softness of polymeric microspheres varies from highly soft hydrogels (elastic modulus: ~ several tens of kPa),[6] to elastomers (elastic modulus: ~ several hundreds of kPa),[7] and rigid polymers (elastic modulus: ~ several GPa).[8] Hydrogel microspheres, i.e., pNA(x) microgels (x = molar ratio of cross-linker in the polymerization feed) were synthesized from *N*-isopropyl acrylamide (NIPAm), acrylic acid (AAc, 10 mol.%), and the cross-linker *N*,*N*'-methylenebis(acrylamide) (BIS; 1, 3, or 5 mol.%) by aqueous free-radical precipitation polymerization[9] (Table S1a). Elastomeric poly(ethyl acrylate) (pEA; T_g ~ −8 °C),[10] as well as rigid poly(methyl methacrylate) (pMMA; T_g ~ 105 °C)[10] and polystyrene (pSt; T_g ~ 107 °C)[10] microspheres with different glass-transition temperatures (T_g) were synthesized by soap-free emulsion polymerization (Table S1b). Initially, we examined the effect of the electrostatic interactions on the adsorption behavior between the microspheres and negatively or positively charged substrates in aqueous solution (Table S1c; Figures S1-3). For this purpose, freshly cleaved negatively charged mica substrates, or a mica substrates treated with 3-aminopropyltriethoxysilane (APTES), which are expected to exhibit positive net charges (AP mica),[11] were used in this study. We found that electrostatic attractions between the

microspheres and the substrates are necessary to adsorb the microspheres on the substrates.

To observe the real-time adsorption behavior of negatively charged microspheres by HS-AFM, a positively charged AP mica was initially monitored by HS-AFM in water (80 μL). Then, part of the water (8 μL) was removed, and a dispersion of microspheres (0.1 wt%, 8 μL) was injected; the dispersion was thoroughly distributed in the water by repeated pipetting during the recording of the images (Scheme 1).

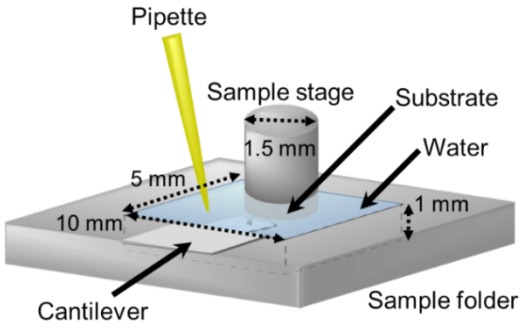

Scheme 1. Schematic illustration of the HS-AFM sample folder.

After the injection of the microgel or elastomeric microsphere dispersions, microspheres appeared in the HS-AFM images, and the number of adsorbed microspheres increased with time up to saturation (Figure 1 and Movie S1-2). On the other hand, after the injection of the rigid pMMA or pSt microsphere dispersions, the microspheres diffused on the surface but were not bound onto the surface (Movie S3).

To quantitatively evaluate the observed adsorption behavior, the number of adsorbed microspheres within a 1500 × 1500 nm^2 area of the HS-AFM images was counted and plotted as a function of time. Figure 2 shows the number of microspheres adsorbed on the substrates. Here, the number is normalized by the saturated number and the adsorption rate is simply estimated from dividing the saturated number of microspheres with the time required for the saturation. The adsorption rate of the pNA(5) microgels with higher cross-linking density (0.58 s^{-1}) was lower than that of the pNA(3) (1.11 s^{-1}) and the pNA(1) (1.98 s^{-1}) microgels with lower cross-linking densities, or that of the elastomeric pEA microspheres (0.24 s^{-1}) (Figure 2), indicating that the adsorption rate of the microgels decreases with increasing cross-linking density. A significant effect of the size of the microgels on their adsorption behavior was not observed under the applied experimental conditions (Figure S4). These results suggest that the adsorption rate cannot be rationalized exclusively by electrostatic interactions, i.e., the adsorption behavior of the microspheres may be controlled by their deformability on the substrate rather than by their electrophoretic mobility (EPM). This indicates that the adsorption rate should be determined by the balance between the electrostatic interactions and the deformability of the microspheres.

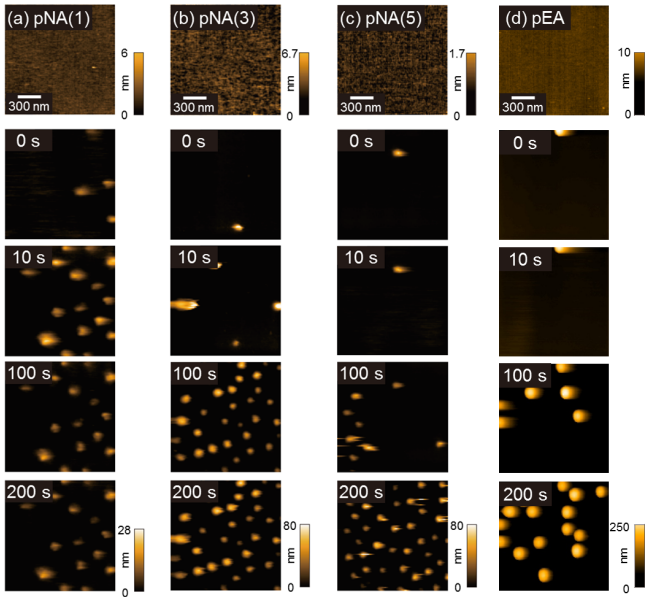

Figure 1. HS-AFM images of the time-dependent adsorption of microgels with different cross-linking densities and elastomeric pEA microspheres onto AP mica substrates: (a) pNA(1), (b) pNA(3), (c) pNA(5), and (d) pEA; [microspheres] = 0.01 wt%; pixel: 120 × 120; scan range: 1500 × 1500 nm^2; frame rate: 1 fps.

To confirm the effect of the deformability of individual microspheres on the adsorption kinetics, we evaluated the height (h) of the adsorbed microspheres from the HS-AFM images immediately after the adsorption on the substrate (Figure S5), while the hydrodynamic diameters (D_h) of the microspheres were estimated based on dynamic light scattering (DLS) measurements. The degree of deformation induced immediately after the adsorption on the substrate was then defined as D_h/h. Figure 3 shows the plots of the correlation between the adsorption rate and D_h/h of the microspheres. For all microgels, the degrees of deformation were > 1 immediately after adsorption (Figure 3 and Table S1a), indicating that all microgels immediately deformed on the substrate. The degree of deformation of the pNA(5) microgels with a high cross-linking density (D_h/h = 2.2) was lower than those of the pNA(3) (D_h/h = 2.9) and the pNA(1) (D_h/h = 16.7) microgels with lower cross-linking densities. Furthermore, the degree of deformation immediately after adsorption affects the net adsorption rate of the microgels onto the substrate (Figure 3). On the other hand, the degrees of deformation of the elastomeric pEA microspheres were ≈ 1 (Figure 3 and Table S1b), indicating that these microspheres should not be deformed on the substrate as much as the microgels.

According to the JKR theory,[12] the total adhesion energy (E_0) of two surfaces in equilibrium contact under zero load is given by $E_0 = -1.2\pi a_0^2\gamma$, whereby $a_0 = (12\pi R^2\gamma/K)^{1/3}$.[13] Here, γ represents the interfacial energy, a_0 the contact radius between the spheres and the surface, while R and K are the radius and the elastic modulus of a sphere, respectively. In the case of rigid microspheres without obvious deformation, the adsorption energy of the microspheres on the solid surface should be very small, given by that the contact radius of the microspheres is small due to the large elastic modulus. Hence, rigid microspheres can desorb immediately after the adsorption onto the substrate. In contrast, soft and deformable microgels with a small elastic modulus deform rapidly and collapse on the surface after getting in contact with the surface. This rapid and drastic deformation provides a relatively large adsorption

energy to the microspheres, as the contact radius of the adsorbed microgels increases rapidly. Thus, the adsorption rate should be dominated by the instantaneous deformability immediately after the adsorption onto the substrate.

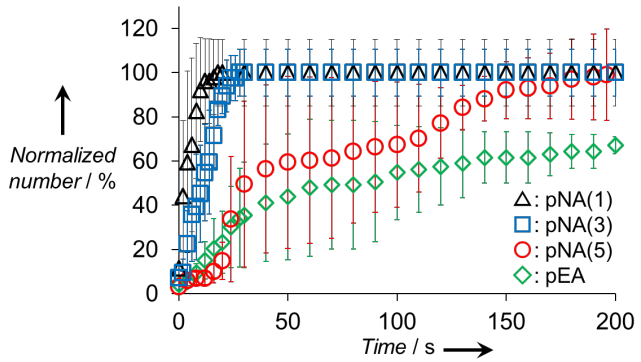

Figure 2. Normalized number of adsorbed microgels with different cross-linking densities and of elastomeric pEA microspheres as a function of time ($N = 3$).

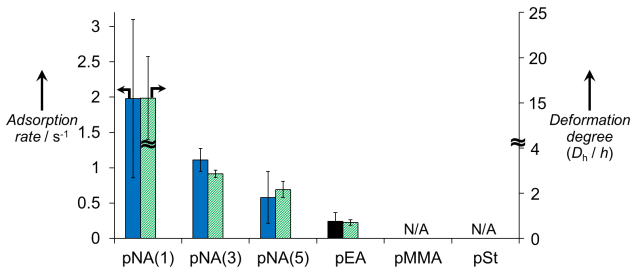

Figure 3. The adsorption rate of microspheres obtained from HS-AFM images ($N = 3$; left axis and left bar), and the degree of deformation (D_h/h) of the polymeric microspheres immediately after the adsorption onto the substrate in aqueous solution ($N = 15$; right axis and right bar).

In conclusion, the effect of the deformability of individual polymeric microspheres on the adsorption kinetics on solid surfaces was examined by monitoring the adsorption processes of microspheres onto solid surfaces in aqueous solution using HS-AFM. The adsorption rates in the presence of electrostatic attractions greatly depend on the deformability of the microspheres, and the adsorption rate decreases in the order pNA(1) > pNA(3) > pNA(5) > pEA, suggesting that highly deformable microgels with a low cross-linking density adsorb faster than elastomeric or rigid microspheres. This result should lead to the development of new design guidelines for polymeric microspheres with applications in biomaterials such as drug delivery vehicles that are focused on the "softness" of the microspheres, as it may allow effective adsorption on target sites under blood flow conditions.

Acknowledgements

D.S., T.U., and S.M. would like to acknowledge Grants-in-Aid for Scientific Research on Innovative Areas from the Japanese Ministry of Education, Culture, Sports, Science, and Technology (MEXT; 26102517 and 16H00760 to D.S.; 26102515 and 16H00758 to T.U.), a grant-in-aid from the Iketani Science and Technology Foundation (0281027-A to D.S.), and a Sasakawa Scientific Research Grant from the Japan Science Society (28-318 to S.M.).

Keywords: polymeric microspheres • microgels • high-speed atomic force microscopy • adsorption • deformability

[1] a) Z. Adamczyk, P. Warszyński, *Adv. Colloid Interface Sci.* **1996**, *63*, 41-149; b) Z. Adamczyk, *Adv. Colloid Interface Sci.* **2003**, *100-102*, 267-347.

[2] Z. Adamczyk, M. Nattich-Rak, M. Sadowska, A. Michna, K. Szczepaniak, *Colloids Surf., A* **2013**, *439*, 3-22.

[3] T. J. Merkel, S. W. Jones, K. P. Herlihy, F. R. Kersey, A. R. Shields, M. Napier, J. C. Luft, H. Wu, W. C. Zamboni, A. Z. Wang, J. E. Bear, J. M. DeSimone, *Proc. Natl. Acad. Sci. USA* **2011**, *108*, 586-591.

[4] a) C. A. Johnson, A. M. Lenhoff, *J. Colloid Interface Sci.* **1996**, *179*, 587-599; b) J. Wiedemair, M. J. Serpe, J. Kim, J. Masson, L. A. Lyon, B. Mizaikoff, C. Kranz, *Langmuir* **2007**, *23*, 130-137; c) S. Höfl, L. Zitzler, T. Hellweg, S. Herminghaus, F. Mugele, *Polymer* **2007**, *48*, 245-254; d) A. Burmistrova, M. Richter, M. Eisele, C. Üzüm, R. Klitzing, *Polymers* **2011**, *3*, 1575-1590; e) A. Mourran, Y. Wu, R. A. Gumerov, A. A. Rudov, I. I. Potemkin, A. Pich, M. M. Möller, *Langmuir* **2016**, *32*, 723-730.

[5] a) T. Ando, T. Uchihashi, T. Fukuma, *Prog. Surf. Sci.* **2008**, *83*, 337-437; b) T. Ando, T. Uchihashi, S. Scheuring, *Chem. Rev.* **2014**, *114*, 3120-3188.

[6] A. B. Imran, K. Esaki, H. Gotoh, T. Seki, K. Ito, Y. Sakai, Y. Takeoka, *Nat. Commun.* **2014**, *5*, 1-8.

[7] J. Sawada, D. Aoki, S. Uchida, H. Otsuka, T. Takata, *ACS Macro Lett.* **2015**, *4*, 598-601.

[8] C. Ishiyama, Y. Higo, *J. Polym. Sci. Part B: Polym. Phys.* **2002**, *40*, 460-465.

[9] a) R. H. Pelton, P. Chibante, *Colloids Surf.* **1986**, *20*, 247-256; b) R. Pelton, *Adv. Colloid Interface Sci.* **2000**, *85*, 1-33.

[10] E. Penzel, J. Rieger, H. A. Schneider, *Polymer* **1997**, *38*, 325-337.

[11] Y. Lyubchenko, L. S. Shlyakhtenko, T. Ando, *Methods* **2011**, *54*, 274-283.

[12] a) K. L. Johnson, K. Kendall, A. D. Roberts, *Proc. R. Soc. London A* **1971**, *324*, 301-313; b) J. M. Y. Carrilla, E. Raphael, A. V. Dobrynin, *Langmuir* **2010**, *26*, 12973-12979; c) H. J. Butt, J. T. Pham, M. Kappl, *Curr. Opin. Colloid Interface Sci.* **2017**, *27*, 82-90.

[13] J. Israelachvili, *Intermolecular and Surface Forces*; Academic Press: London, **1992**.

Supporting Information

Table of Contents

Experimental Procedures

Materials

N-isopropylacrylamide (NIPAm, 98%), *N*,*N*′-methylenebis(acrylamide) (BIS, 97%), acrylic acid (AAc, 99%), ethyl acrylate (EA, 97%), methyl methacrylate (MMA, 98%), styrene (St, 99%), sodium dodecyl sulfate (SDS, 95%), potassium persulfate (KPS, 95%), and 2,2′-azobis(2-methylpropinamidine)dihydrochloride (V-50, 95%) were purchased from Wako Pure Chemical Industries (Japan) and used as received. 3-Aminopropyltriethoxysilane (APTES) was purchased from Shin-Etsu Silicones (Japan). For the synthesis of (4-vinyl-4′-methyl-2,2′-bipyridine)bis(2,2′-bipyridine)bis(hexafluorophosphate) [$Ru(bpy)_3$ cationic monomer], a previously reported method was used.[1] Water for all reactions, including the preparation of solutions and the purification of polymers, was distilled and subsequently subjected to ion exchange (EYELA, SA-2100E1).

Microgel synthesis

Poly(NIPAm-*co*-AAc) (**pNA**) microgels were synthesized by radical precipitation polymerization in aqueous solution. For that purpose, a mixture of NIPAm (1.511 g/89 mol.%, 1.477 g/87 mol.%, or 1.443 g/85 mol.%), BIS (0.024 g/1 mol.%, 0.070 g/3 mol.%, or 0.115 g/5 mol.%), AAc (0.109 g/10 mol.%, 0.108 g/10 mol.%, or 0.108 g/10 mol.%) in water (90 mL) was poured into a three-necked round-bottomed flask (200 mL) equipped with a mechanical stirrer, condenser, and a nitrogen gas inlet. The initial total monomer concentration (150 mM) was maintained. To remove any oxygen, the monomer solution was heated to 70 °C in an oil bath under nitrogen sparging (30 min) and constant stirring (250 rpm). After stabilizing the solution for 30 min, SDS (0.115 g/4 mM, 0.115 g/4 mM, or 0.115 g/4 mM) was dissolved in water (5 mL) and added to the flask. Then, KPS (0.054 g/2 mM, 0.054 g/2 mM, or 0.054 g/2 mM) dissolved in water (5 mL) was added to the flask in order to initiate the polymerization. After stirring for 4 h, the dispersion was cooled to room temperature. The obtained microgels were purified twice by the following procedure: centrifugation (415 000 *g* / 15 °C), decantation of the supernatant, and redispersion

of the precipitate in water. The dispersion was then dialyzed for 5 days, whereby the water was changed daily. The microgels were denoted as **pNA(1)**, **pNA(3)**, or **pNA(5)**, whereby the numbers in parentheses refer to the mole percentage of BIS in the polymerization feed.

PolyNIPAm (**pN**) microgels were synthesized by radical precipitation polymerization in aqueous solution. A mixture of NIPAm (1.681 g, 99 mol.%) and BIS (0.023 g, 1 mol.%) in water (90 mL) was poured into a three-necked round-bottomed flask (200 mL) equipped with a mechanical stirrer, condenser, and a nitrogen gas inlet. The solution was purged as described above. After stabilization for 30 min, SDS (0.058 g, 2 mM) dissolved in water (5 mL) was added to the flask, and polymerization was initiated by adding KPS (0.054 g, 2 mM) in water (5 mL). The dispersion was stirred for 4 h and cooled to room temperature. The thus obtained microgels were purified as described above. The dispersion was then dialyzed for 4 days, whereby the water was changed daily.

Cationic poly(NIPAm-*co*-Ru(bpy)$_3$) (**pNRu**) microgels were synthesized by radical precipitation polymerization in aqueous solution. A mixture of NIPAm (0.224 g, 88 mol.%), BIS (0.035 g, 10 mol.%), and Ru(bpy)$_3$ (0.041 g, 2 mol.%) in water (28 mL) was poured into a three-necked round-bottomed flask (50 mL) equipped with a mechanical stirrer, condenser, and a nitrogen gas inlet. The initial total monomer concentration (75 mM) was maintained. After purging the solution as described above and stabilization (30 min), the polymerization was initiated by addition of V-50 (0.016 g, 2 mM) in water (2 mL). The dispersion was stirred for 4 h, and then cooled to room temperature. The thus obtained microgels were purified as described above. The dispersion was then dialyzed for 2 days, whereby the water was changed daily.

Synthesis of elastomeric microspheres

Poly(ethyl acrylate) (**pEA**) microspheres were synthesized by surfactant-free emulsion polymerization. EA (3.008 g, 100 mol.%) in water (95 mL) was poured into a three-necked round-bottomed flask (200 mL) equipped with a mechanical stirrer, condenser, and a nitrogen gas inlet. The initial total monomer concentration (300 mM) was maintained. To remove any oxygen from the solution,

it was heated to 70 °C in an oil bath under nitrogen sparging (30 min) and constant stirring (300 rpm). After stabilization for 30 min, KPS (0.054 g, 2 mM) in water (5 mL) was added to initiate the polymerization. The dispersion was stirred for 24 h, cooled to room temperature, and then dialyzed for 7 days, whereby the water was changed daily.

Synthesis of rigid microspheres

Poly(methyl methacrylate) (**pMMA**) and polystyrene (**pSt**) microspheres were synthesized by surfactant-free emulsion polymerization. MMA (10.012 g, 100 mol.%) or St (5.2075 g, 100 mol.%) in water (95 mL) was poured into a three-necked round-bottomed flask (200 mL) equipped with a mechanical stirrer, condenser, and a nitrogen gas inlet. The initial total monomer concentration (MMA: 1000 mM; St: 500 mM) was maintained. After removing oxygen from the solutions as described for **pEA** and stabilization for 30 min, KPS (0.054 g, 2 mM) in water (5 mL) was added to initiate the polymerizations. The dispersions were stirred for 24 h, cooled to room temperature, and dialyzed for 7 days, whereby the water was changed daily.

Dynamic light scattering (DLS) measurements

The hydrodynamic diameters of the microspheres in aqueous solution were estimated by dynamic light scattering (DLS; Malvern Instruments Ltd.; ZetasizerNanoS). The DLS data represent averages of three individual measurements of 15 consecutive runs of the intensity autocorrelation (acquisition time: 30 s). The concentration of the microspheres in the DLS experiments was approximately 0.001 wt%. Before the measurements, the samples were allowed to thermally equilibrate at 25 °C for 5 min. The time-dependent scattering intensity was detected at a total scattering angle of 173° (refractive index n = 1.33). The hydrodynamic diameters of the microspheres were calculated from the measured diffusion coefficients using the Stokes–Einstein equation (Zetasizer software v6.12).

Electrophoretic mobility (EPM)

The electrophoretic mobilities (EPMs) of the microspheres were determined by a Zetasizer NanoZS system (Malvern, Zetasizer software Ver. 4.20). The EPM data represent averages of three individual measurements of 20 consecutive runs. Before the measurements, the samples were allowed to thermally equilibrate at 25 °C for 5 min. The microgel concentration in the measurements was approximately 0.01 wt%, and the concentration of the elastomeric or rigid microspheres was approximately 0.001 wt% in pure water.

HS-AFM observations

A laboratory-built HS-AFM was used in this study, and the instrument has previously been described elsewhere.[2] All images and movies shown in this paper were acquired in the tapping mode, in which a cantilever (length: 6–7 μm; width: 2 μm; thickness: 90 nm) oscillates near a mechanical resonance. The cantilever oscillation was detected by an optical-beam-deflection detector with a red laser (650 nm). Typical values for the spring constant, resonant frequency, and quality factor in aqueous solution of this cantilever are ~0.1 N/m, ~600 kHz, and ~2, respectively. An amorphous carbon tip was grown on the original bird-beak tip by electron beam deposition, and the carbon tip was subsequently sharpened (radius: ~4 nm) by plasma etching under an argon atmosphere. For the HS-AFM imaging of polymeric microspheres, the cantilever free-oscillation amplitude was set to 5~30 nm, and the set-point amplitude was set to 70-90% of the free-oscillation amplitude depending on the microsphere size. In order to modify the electric properties of the mica surfaces, these were chemically modified with 3-aminopropyltriethoxysilane (APTES), which leads to the formation of positively charged surfaces.[3] For that purpose, an APTES-diluted aqueous solution (1 wt%; 3 μL) was dropped on a freshly cleaved mica surface, and the substrate was incubated for 3 min at room temperature. After the incubation, the mica surface was rinsed with pure water to remove any excess APTES. The adsorption behavior of the microspheres on the APTES-treated mica substrates (AP mica) was observed by removing 8 μL of water from the observation solution (80 μL pure water) and replacing it with the same volume of a microsphere

dispersion (0.1 wt%) during the recording of the images. All HS-AFM imaging was performed at room temperature (~25 °C) under the following conditions: scanning area = 1500 × 1500 nm^2; 120 ×120 $pixels^2$; frame rate = 1 fps.

Results and Discussion

Table S1 (a). Chemical composition, hydrodynamic diameters (D_h), and electrophoretic mobility (EPM) of the microgels measured in pure water, as well as the degree of deformation of the microgels in aqueous solution (D_h/h).

	NIPAm (mol.%)	BIS (mol.%)	AAc (mol.%)	D_h (nm)	EPM (10^{-8} $m^2V^{-1}s^{-1}$)	D_h/h
pNA(1)	89	1	10	378 ± 12	−2.50 ± 0.13	16.7 ± 4.9
pNA(3)	87	3	10	257 ± 5	−2.74 ± 0.18	2.9 ± 0.8
pNA(5)	85	5	10	242 ± 14	−2.88 ± 0.24	2.2 ± 0.7

Table S1 (b). Chemical composition, hydrodynamic diameters (D_h), and electrophoretic mobility (EPM) of the elastomeric and rigid microspheres measured in pure water, as well as the degree of deformation of the microspheres in aqueous solution (D_h/h).

	EA (mol.%)	MMA (mol.%)	St (mol.%)	D_h (nm)	EPM (10^{-8} $m^2V^{-1}s^{-1}$)	D_h/h
pEA	100	0	0	198 ± 1	−2.49 ± 0.02	0.7 ± 0.1
pMMA	0	100	0	402 ± 2	−3.24 ± 0.12	N/A
pSt	0	0	100	250 ± 2	−1.76 ± 0.03	N/A

Table S1 (c). Chemical composition, hydrodynamic diameters (D_h), and electrophoretic mobility (EPM) of weakly anionic and cationic microgels measured in pure water.

	NIPAm (mol.%)	BIS (mol.%)	$Ru(bpy)_3$ (mol.%)	D_h (nm)	EPM (10^{-8} $m^2V^{-1}s^{-1}$)
pN	99	1	0	226 ± 2	−0.64 ± 0.04
pNRu	88	10	2	166 ± 9	+1.90 ± 0.10

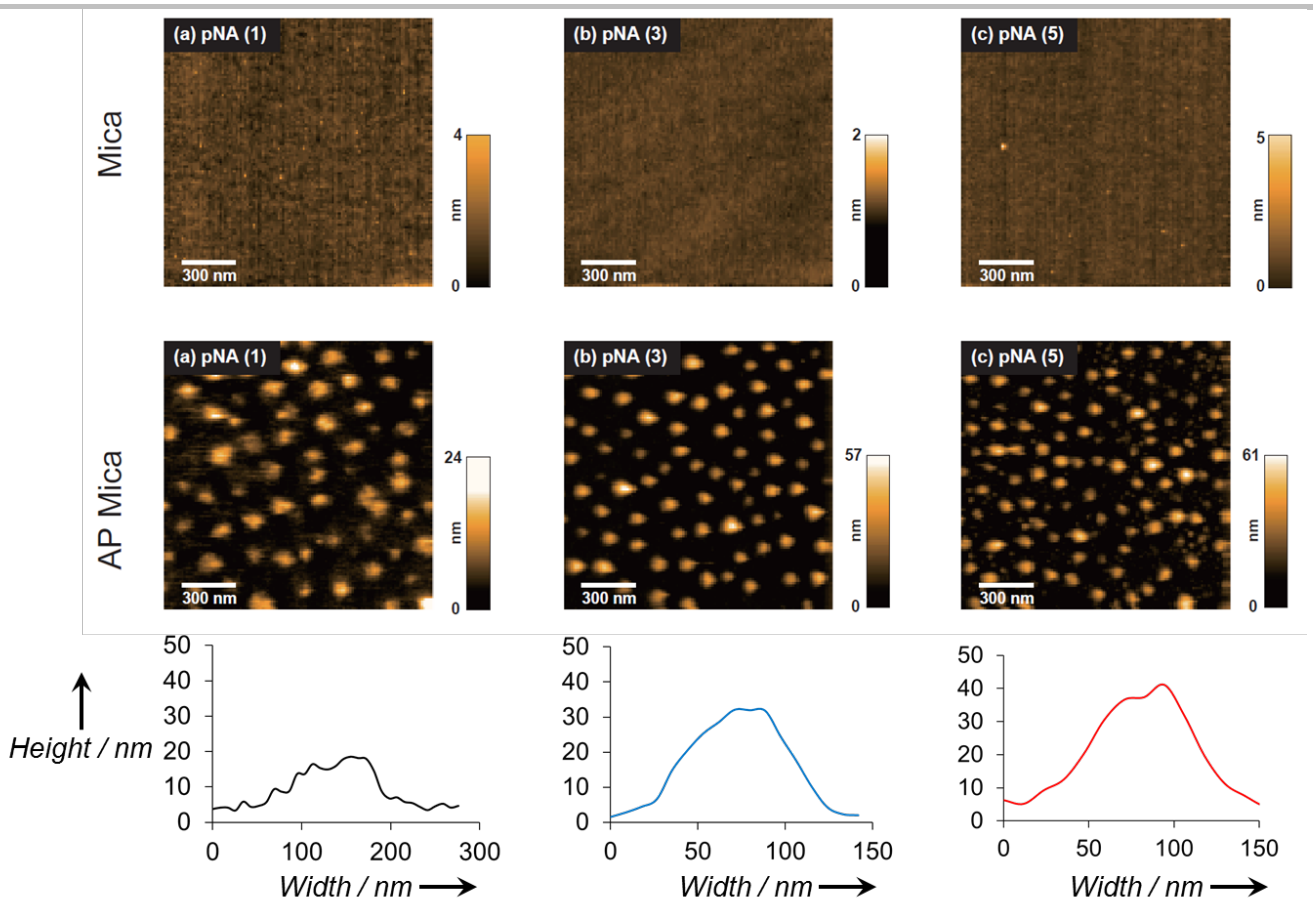

Figure S1. HS-AFM images of (a) pNA(1), (b) pNA(3), and (c) pNA(5) microgels adsorbed onto different substrates (mica or AP mica) in pure water, and typical height profiles of adsorbed microgels. A microgel dispersion (3 µL; 0.1 wt%) was dropped onto the surface of freshly cleaved mica or AP mica substrates, and incubated for 5 min at room temperature. The substrate was then rinsed with pure water to remove any non-adsorbed microgel and placed in the sample folder (filled with 80 µL water). The HS-AFM measurement was performed at room temperature. Pixels: 120 × 120; scan range: 1500 × 1500 nm^2; frame rate: 1 fps. Anionic pNA microgels did not adsorb onto the negatively charged mica substrates, while they adsorbed onto the positively charged AP mica substrates.

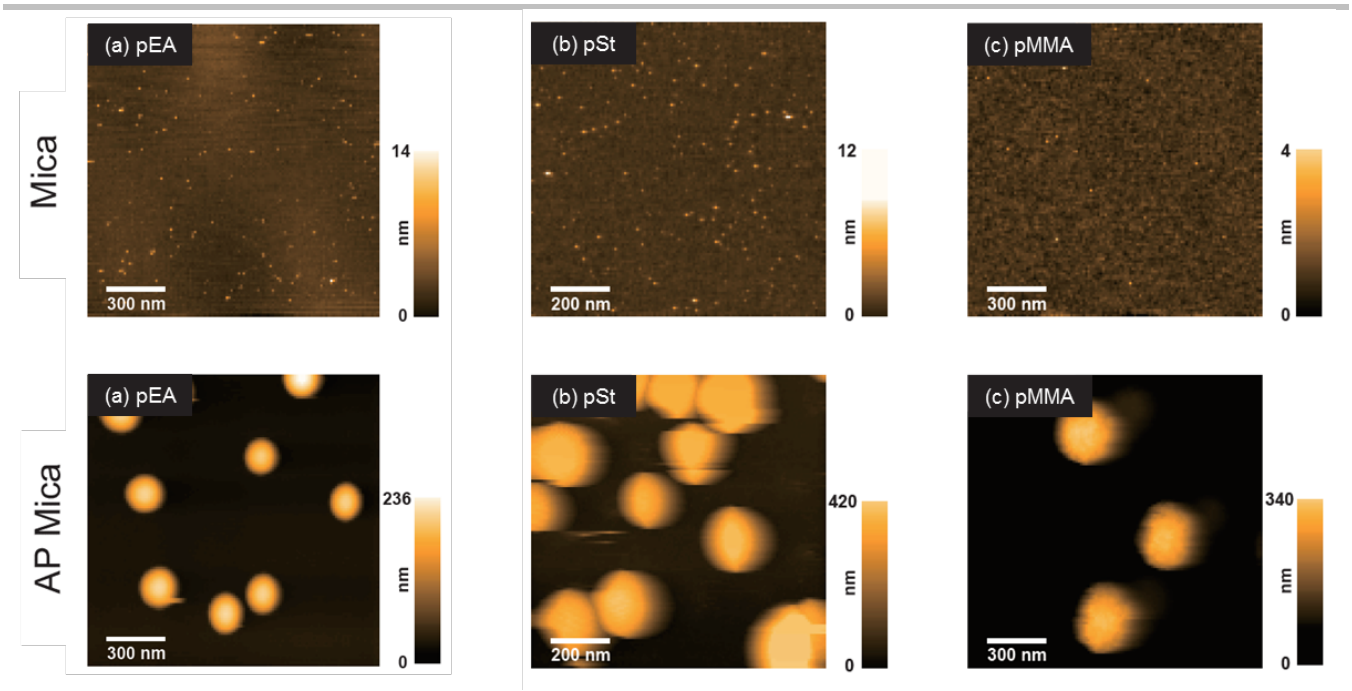

Figure S2. HS-AFM images of adsorbed (a) anionic pEA, (b) pSt, and (c) pMMA microspheres in pure water using different substrates (mica or AP mica). Anionic pEA, pSt, and pMMA microspheres did not adsorb onto the negatively charged mica substrates, while they adsorbed onto the positively charged AP mica substrates.

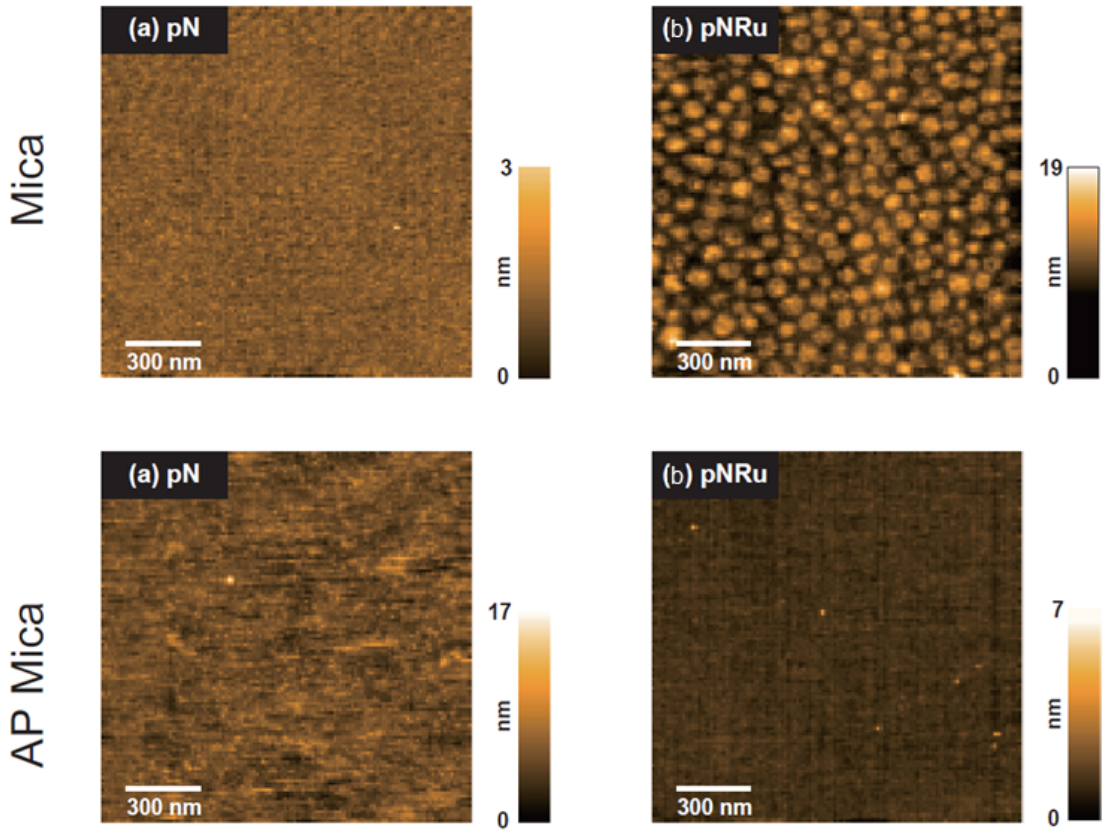

Figure S3. HS-AFM images of adsorbed (a) weakly anionic pN and (b) cationic pNRu microgels in pure water using different substrates (mica or AP mica). Weakly anionic pN microgels did not adsorb onto the negatively charged mica or positively charged AP mica substrates. Cationic pNRu microgels adsorbed onto the negatively charged mica substrates, while they did not adsorb onto the positively charged AP mica substrates.

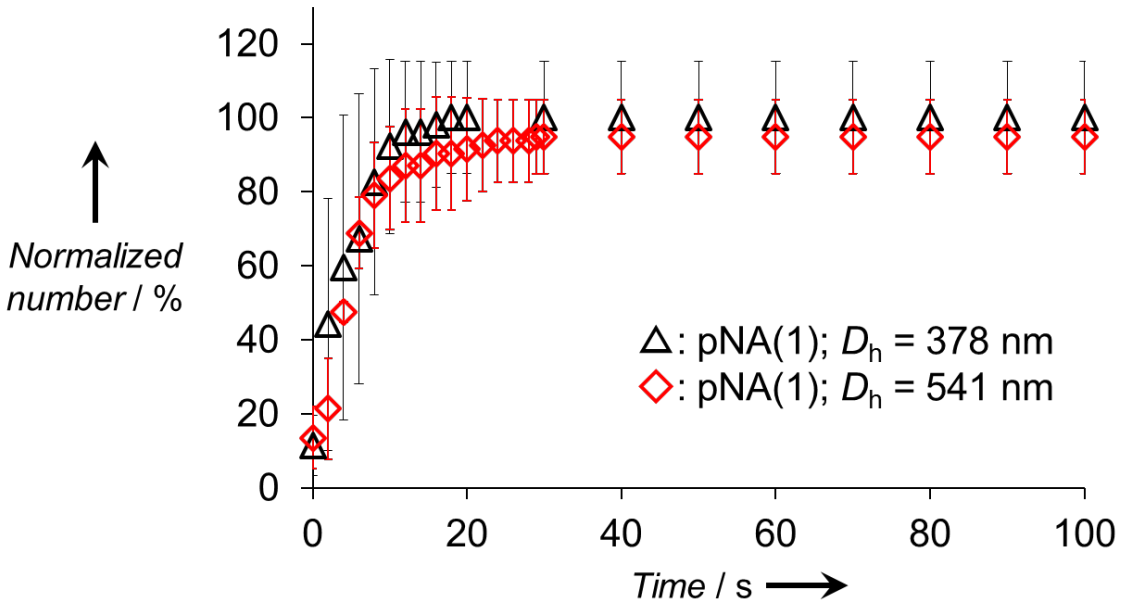

Figure S4. Normalized number of adsorbed microgels with different size (D_h = 378 nm and D_h = 541 nm; difference in volume by a factor of ~2.9) as a function of time (N = 3). The adsorption behavior of these microgels is comparable.

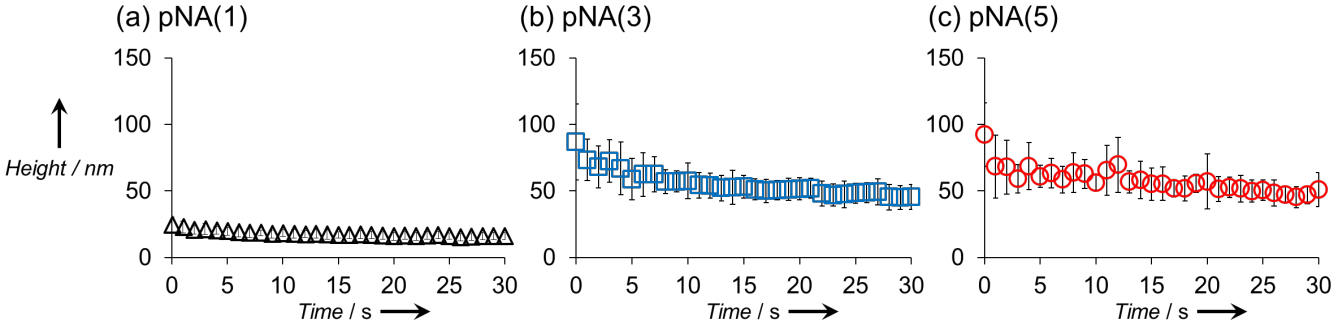

Figure S5. Time-dependence of the height profiles of the pNA microgels after the adsorption onto the substrates (0 -30 s). (a) pNA(1), (b) pNA(3), and (c) pNA(5) microgels. The height of all adsorbed pNA microgels immediately after the adsorption (just appeared on the image, 0 s) is much smaller than the hydrodynamic diameter in water, indicating high deformation on the substrate. After that, the height of the adsorbed microgels decreased and reached almost an equilibrium state.

Supporting Movies

Movie S1. HS-AFM movies of the adsorption behavior of pNA microgels on AP mica substrates (10× speed): (a) pNA(1), (b) pNA(3), and (c) pNA(5) microgels.

Movie S2. HS-AFM movies of the adsorption behavior of elastomeric pEA microspheres on AP mica substrates (30× speed).

Movie S3. HS-AFM movies of the adsorption behavior of rigid pMMA and pSt microspheres on AP mica substrates: (a) pMMA (10× speed) and (b) pSt (30× speed).

References

[1] P. K. Ghosh, T. G. Spiro, *J. Am. Chem. Soc.* **1980**, *102*, 5543–5549.
[2] T. Ando, T. Uchihashi, T. Fukuma, *Prog. Surf. Sci.* **2008**, *83*, 337–437.
[3] Y. Lyubchenko, L. S. Shlyakhtenko, T. Ando, *Methods* **2011**, *54*, 274–283.